

AD-A193 840

COMPUTER-CONTROLLED MEASUREMENTS OF NONLINEAR STANDING WAVES(U) NAVAL POSTGRADUATE SCHOOL MONTEREY CA
H BASARAN DEC 87

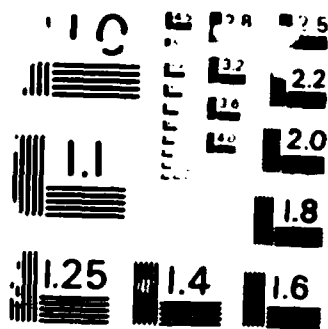
1/1

H BASARAN DEC 87

UNCLASSIFIED

F/G 20/1

44



RESOLUTION TEST CHART
 NATIONAL BUREAU OF STANDARDS-1963-A

AD-A193 840

DTIC FILE COPY

2

NAVAL POSTGRADUATE SCHOOL

Monterey, California



THESIS

DTIC
ELECTE
JUN 03 1988
S H D

COMPUTER-CONTROLLED MEASUREMENTS OF
NONLINEAR STANDING WAVES

by

Hakan Basaran

December 1987

Thesis Advisor

J. V. Sanders

Approved for public release; distribution is unlimited.

REPORT DOCUMENTATION PAGE

1a REPORT SECURITY CLASSIFICATION Unclassified		1b RESTRICTIVE MARKINGS	
2a SECURITY CLASSIFICATION AUTHORITY		3 DISTRIBUTION AVAILABILITY OF REPORT Approved for public release; distribution is unlimited.	
2b DECLASSIFICATION/DOWNGRADING SCHEDULE			
4 PERFORMING ORGANIZATION REPORT NUMBER(S)		5 MONITORING ORGANIZATION REPORT NUMBER(S)	
6a NAME OF PERFORMING ORGANIZATION Naval Postgraduate School	6b OFFICE SYMBOL (if applicable) 33	7a NAME OF MONITORING ORGANIZATION Naval Postgraduate School	
6c ADDRESS (City, State, and ZIP Code) Monterey, California 93946-5000		7b ADDRESS (City, State, and ZIP Code) Monterey, California 93946-5000	
8a NAME OF FUNDING SPONSORING ORGANIZATION	8b OFFICE SYMBOL (if applicable)	9 PROCUREMENT INSTRUMENT IDENTIFICATION NUMBER	
8c ADDRESS (City, State, and ZIP Code)		10 SOURCE OF FUNDING NUMBERS	
		PROGRAM ELEMENT NO	PROJECT NO TASK NO WORK UNIT ACCESSION NO
11 TITLE (Include Security Classification) Computer-Controlled Measurements of Nonlinear Standing Waves			
12 PERSONAL AUTHOR(S) Basaran, Hakan			
13a TYPE OF REPORT Master's Thesis	13b DATE COVERED FROM TO	14 DATE OF REPORT (Year, Month, Day) 1987-12-01	15 PAGE COUNT 55
16 SUPPLEMENTARY NOTES			
17 COSAT CODE FIELD GROUP SUBGROUP		18 SUBJECT TERMS (Continue on reverse if necessary and identify by block number) Standing waves Nonlinearity	
19 ABSTRACT (Continue on reverse if necessary and identify by block number) A computer-controlled data collection system was designed and implemented to analyze finite amplitude acoustic standing waves in a rectangular air-filled cavity with linear and wedge-shaped boundary perturbations. The response of a nonlinear standing wave in perturbed and unperturbed cavities was studied. The experimental results showed that the computer-obtained data was in qualitative agreement with that previously obtained by manual procedures. Quantitative comparisons with theory could not be made because the properties of the cavity did not match those for which theoretical predictions are available.			
20 DISTRIBUTION AVAILABILITY OF ABSTRACT <input checked="" type="checkbox"/> UNCLASSIFIED UNLIMITED <input type="checkbox"/> SAME AS RPT <input type="checkbox"/> DTIC USERS		21 ABSTRACT SECURITY CLASSIFICATION Unclassified	
22a NAME OF RESPONSIBLE INDIVIDUAL J. V. Sanders		22b TELEPHONE (Include Area Code) (408) 933-0813	22c OFFICE SYMBOL 6100

Approved for public release; distribution is unlimited.

**Computer-Controlled Measurements of
Nonlinear Standing Waves**

by

Hakan Basaran
Lieutenant Junior Grade, Turkish Navy
B.S., Turkish Naval Academy, 1981

Submitted in partial fulfillment of the
requirements for the degree of

MASTER OF SCIENCE IN ENGINEERING ACOUSTICS

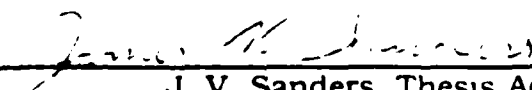
from the

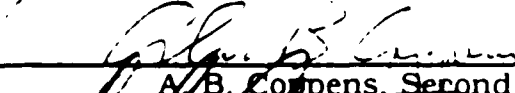
NAVAL POSTGRADUATE SCHOOL
December 1987


Author:


Hakan Basaran


Approved by:


J. V. Sanders, Thesis Advisor


A. B. Compens, Second Reader


S. L. Garrett, Chairman,

Engineering Acoustics Academic Group


Gordon Schacher, Dean,
Engineering and Sciences

ABSTRACT

A computer-controlled data collection system was designed and implemented to analyze finite amplitude acoustic standing waves in a rectangular air-filled cavity with linear and wedge-shaped boundary perturbations. The response of a nonlinear standing wave in perturbed and unperturbed cavities was studied. The experimental results showed that the computer-obtained data was in qualitative agreement with that previously obtained by manual procedures. Quantitative comparisons with theory could not be made because the properties of the cavity did not match those for which theoretical predictions are available.



Accession For	
NTIS	<input checked="checked" type="checkbox"/>
DTIC TAB	<input type="checkbox"/>
Unannounced	<input type="checkbox"/>
Justification	<input type="checkbox"/>
By	
In	
Approved For	
Dist	
A-1	

TABLE OF CONTENTS

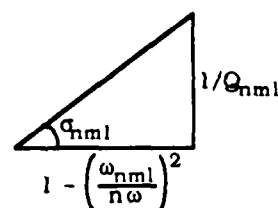
I. INTRODUCTION	10
II. BACKGROUND AND THEORY	11
III. EXPERIMENTAL CONSIDERATIONS	20
A. COMPUTER-CONTROLLED APPARATUS	20
B. STRENGTH PARAMETER AND MICROPHONE SENSITIVITY	24
C. FREQUENCY PARAMETER	25
D. HARMONICITY COEFFICIENT	25
E. COMPUTER PROGRAMS	26
IV. DATA COLLECTION PROCEDURES	29
A. SYSTEM ALIGNMENT	29
B. AUTOMATIC DATA COLLECTION	29
1. Pre-Run and Post-Run Infinitesimal Amplitude Measurements	30
2. Finite Amplitude Measurement	32
V. RESULTS	34
VI. CONCLUSIONS	36
APPENDIX A CURVES	37

APPENDIX B	TABLES	40
APPENDIX C	COMPUTER PROGRAMS	47
LIST OF REFERENCES		52
INITIAL DISTRIBUTION LIST		54

LIST OF SYMBOLS

ρ	Instantaneous density of the fluid
ρ_0	Equilibrium density of the fluid
Φ	Velocity potential
$\vec{u} = \nabla \Phi$	Particle velocity
s	Condensation
∇	Gradient operator
$\nabla \cdot$	Divergence operator
$\nabla \times$	Curl operator
∇^2	Laplacian operator
$\gamma = C_p/C_v$	Ratio of specific heats
C_0	Speed of sound in an unbounded volume of air
P	Instantaneous total pressure
P_0	Equilibrium total pressure
$p = P - P_0$	Acoustic pressure
$\nabla^2 = \nabla^2 - \frac{\partial^2}{\partial t^2}$	D'Lambertian operator
∇_L^2	D'Lambertian operator with losses
$C_0^2 = \left(\frac{\partial P}{\partial \rho} \right)_{\rho=\rho_0}$	Speed of sound in air
R_n	Fourier coefficient of n^{th} harmonic component

ϕ_n	Phase angle of the n^{th} harmonic component where $\phi_1 = 0$
F_n	$2Q_n \left(\frac{n\omega - \omega_n}{\omega_n} \right)$
θ_n	Arctan $(-F_n)$
ω_n	Resonance angular frequency
ω	Driving angular frequency (near ω_1)
$\omega_{nu} - \omega_{nL}$	Bandwidth at half power
N	$1/2$ for a one-dimensional standing wave $1/4$ for a two-dimensional standing wave $1/8$ for a three-dimensional standing wave
M	Mach number = $\frac{P_1}{\rho_0 C_0^2}$
β	$(\gamma + 1)/2$ for a gas
$(n,m,l/\omega,\theta)$	A standing wave designation when the (n,m,l) mode is driven at angular frequency ω ; θ is the phase angle with respect to fundamental
L_x, L_y, L_z	The dimensions of the cavity
a_{nl}	Fourier coefficients
F_{nml}	$\cot \sigma_{nml}$
σ_{nml}	Angle defined as:



Q_{nml}	Quality factor of the given mode
S_{nml}	$\frac{Q_{nml}}{\sqrt{1+F_{nml}^2}} = Q_{nml} \sin \sigma_{nml}$
RHS	Right-hand side of equation
LHS	Left-hand side of equation
p'	First-order perturbation correction due to boundary irregularities

ACKNOWLEDGMENT

The author wishes to acknowledge the support and encouragement of Professors James V. Sanders and Alan B. Copper³, who not only provided the initial idea for the topic but also provided invaluable assistance throughout the course of the experiment.

Sincere thanks also to Mr. Ender Kuntsal and LT Hans Wolfgang Kuebler for their helpful suggestions on the choice of equipment for this research.

I also wish to thank Professor S. L. Garrett for providing me with research space.

I. INTRODUCTION

A one-dimensional mathematical model for finite-amplitude standing waves in a real cavity was studied by Coppens and Sanders [Refs. 1, 2] in 1968. In 1974, this model was extended to three dimensions. Losses and resonance frequencies, inadequately described by the classical theory of wall losses, are obtained for the real cavity from measurements obtained in the linear acoustic regime. The research done in 1974 showed that when a cavity is driven near the resonance of a standing wave the nonlinear distortion primarily involves only the normal modes of the cavity that are "familiially related" to the driven mode. Lane [Ref. 3], DeVall [Ref. 4], Slocum [Ref.5], and Kuntsal [Ref. 6] examined the problem and showed that experimental results are in excellent agreement with the theory except when a degeneracy exists in the cavity.

The purpose of the research reported in this thesis was to design and implement a computer-assisted data collection and analysis system for measuring the finite-amplitude distortion in a perturbed cavity with degeneracies.

II. BACKGROUND AND THEORY

When the sound intensity in an acoustic process becomes so high that the principle of superposition no longer applies, we enter the domain of nonlinear acoustics. The limits of linear approximations in the equation of force, mass continuity, and state are exceeded and the resultant vibrational disturbance at any point in the medium will no longer be equal to the sum of its individual components. The essence of the nonlinear acoustic mechanism is that an intense wave perturbs the medium in which it exists and this perturbation alters the natural order governing the wave's behavior. The result is that segments of the disturbance in a warmer compression travel faster than those in a cooler rarefaction. When this happens, the acoustical wave alters its shape, steepening as it travels along. The alteration is infinitesimal for weak disturbances and gradually increases in importance with increases in both amplitude and frequency of sound. [Ref. 2]

In 1968, Kirchoff [Ref. 7] studied the distortion of intense acoustic waves in an unbounded fluid. This study was extended by Lamb [Ref. 8], Fay [Ref. 9], and by Keller [Ref. 10].

Keck and Beyer [Ref. 11] approached the problem of unbounded propagation by using perturbation methods and Fourier series representations of the waveform. The model of Coppens and Sanders [Ref. 12] dealt with finite-amplitude standing waves in rigid walled cavities. They extended the Keck-Beyer perturbation approach to include wall losses predicted by the Rayleigh-Kirchoff theory [Ref. 7].

and showed excellent agreement with experiments conducted in a rigid-walled tube at low but finite levels of excitation. The experimental work by Beech [Ref. 13] and by Ruff [Ref. 14] showed that at high excitation levels differences developed between theory and experiment. Experimental work by DeVall [Ref. 4] and by Kilmer [Ref. 15] showed that if degeneracies existed the model failed to account for the experimentally observed excitation of "nonfamilial" modes.

The effects of various geometrical boundary perturbations on a rigid-walled cavity investigated by Aydin [Ref. 16] showed that the standing waves that exist in an ideal cavity must be corrected when the boundaries are irregular. The model of Coppens and Sanders is based on a three-dimensional, nonlinear wave equation with a dissipative term describing absorptive losses encountered by standing waves in rigid walled cavities. As stated in [Ref. 12],

The standing waves which can be excited in any real cavity deviate from predictions of the linear wave equation with ideal boundary conditions for the following reasons:

- a. The presence of boundary-layer losses at the cavity surfaces yields a dispersive contribution to the wave equation.
- b. Geometrical irregularities alter the effective dimensions of the cavity.

Both of these mechanisms can be treated separately as long as the shift in frequency is so small that the actual resonances are close to the theoretical values resulting from the classical model. These are treated by assuming the dimensions are exact, and the apparent phase speeds are determined on that basis.

The resonance frequency for each standing wave is defined as [Ref. 6]

$$\omega_n = C_n [(n_x k_x)^2 + (n_y k_y)^2 + (n_z k_z)^2]^{1/2} \quad (1)$$

where $k_x = \frac{n\pi}{L_x}$, $k_y = \frac{m\pi}{L_y}$, $k_z = \frac{l\pi}{L_z}$, and n , m , and l are integers. C_n is the apparent phase speed appropriate for that frequency.

The force equation, in Eulerian coordinates, can be written in the form

$$\frac{\partial \vec{u}}{\partial t} + (\vec{u} \cdot \nabla) \vec{u} + \frac{1}{\rho} \nabla P = \frac{1}{\rho} \lambda \vec{u} \quad (2)$$

where the operator λ describes those physical processes leading to absorption and dispersion. If we ignore rotational effects so that $\vec{u} = \nabla \phi$, restrict waves to rectangular cavities, and neglect terms of orders higher than M^2 , $M(\alpha/k)$, and $(\alpha/k)^2$, the result is a quadratically nonlinear wave equation [Ref. 12].

$$C_p^2 - \frac{2}{L} \left(\frac{P}{\rho_0 C_0^2} \right) = - \frac{\partial^2}{\partial t^2} \left[\frac{\gamma - 1}{2} \left(\frac{P}{\rho_0 C_0^2} \right)^2 + \left(\frac{u}{C_0} \right)^2 \right] \quad (3)$$

The standing pressure wave in a rectangular cavity has the form [Ref. 12]

$$p = \cos k_x x \cos k_y y \cos k_z z \cos \omega t \quad (4)$$

If the cavity is being driven near resonance, the nonresonant terms contribute almost nothing with respect to the resonant terms. So the standing wave pressure has the form of

$$p = \sum_{n=1}^{\infty} p_n \quad (5)$$

where each P_n is of frequency $n\omega$ and has the form [Ref. 12].

$$\frac{P_n}{(\rho_0 C_0^2)} = MR_n \cos n k_x x \cos n k_y y \cos n k_z z \sin(n\omega t + Q_n) \quad (6)$$

These p_n s constitute those normal modes familiarly related to p_1 .

The nonlinear, coupled, transcendental equations which must be solved for the R_n s are

$$R_n \left\{ \begin{array}{c} \cos \\ \sin \end{array} \right\} (Q_n - \theta_n) = NM\beta Q_n \cos Q_n \left[\frac{1}{2} \sum_{j=1}^{n-1} R_j R_{n-j} \left\{ \begin{array}{c} \cos \\ \sin \end{array} \right\} * (Q_j - Q_{n-j}) \right. \\ \left. - \sum_{j=1}^{\infty} R_{n+j} R_j \left\{ \begin{array}{c} \cos \\ \sin \end{array} \right\} * (Q_{n-j} - Q_j) \right] \quad \text{for all } n > 1 \quad (7)$$

$$R \equiv 1 \quad \text{for } n=1$$

where $Q_n = \text{Arctan}(-F_n)$

$$F_n = Q \left[(n\omega)^2 - (\omega_n)^2 \right] / (n\omega)^2 \doteq 2Q_n \left(\frac{n\omega - \omega_n}{\omega_n} \right) \quad \text{for } \frac{n\omega - \omega_n}{\omega_n} \ll 1 \quad (8)$$

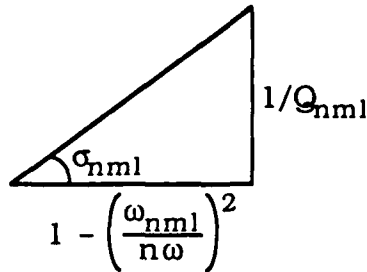
$$Q_n = \frac{\omega_n}{\omega_{nu} - \omega_{nL}} \quad (9)$$

Total pressure near resonance for perturbed boundaries is [Ref. 6]

$$p = (n, m, l/\omega, \theta) - \frac{\epsilon}{\left(\frac{\omega}{C_0}\right)^2 L_x} \sum_{\substack{n=0 \\ m=0 \\ l=0}}^{\infty} a_{nml} \Delta_n (-1)^n *$$

$$S_{nml} (n, m, l/\omega, \theta + \sigma_{nml}) \quad (10)$$

where S_{nml} ~ first-order perturbation correction and σ_{nml} angle which is defined as [Ref. 6]:



$$\epsilon = \frac{\Delta}{L_x}$$

Δ = Amp. of perturbation

If the cavity has perturbed walls, the solution will be in terms of a summation of the classical linear solution for ideal boundaries plus perturbation correction terms due to the irregular boundary:

$$p = p_0 + \epsilon p' + \epsilon^2 p'' + \dots \quad (11)$$

Since the magnitude of the boundary perturbation is kept small, second and higher terms in ϵ can be considered insignificant, so that

$$p = p_0 + \epsilon p' \quad (12)$$

and p must satisfy the following conditions,

$$\frac{\partial^2 p}{\partial L} = 0 \quad (13)$$

and

$$\begin{aligned} \nabla p \cdot \vec{n} &= 0 & \text{at } x &= 0, L_x [1 + \epsilon f(y,z)] \\ & & y &= 0, L_y \\ & & z &= 0, L_z \end{aligned} \quad (14)$$

where \vec{n} , the local normal to the real surface, is obtained by taking the gradient of the equation for the boundary [Ref. 1],

$$\vec{n} = \nabla \{x - L_x [1 + \epsilon f(y,z)]\} \quad (15)$$

Thus, to the first order in ϵ ,

$$\vec{n} = \hat{x} - \epsilon L_x \frac{\partial f(y,z)}{\partial y} \hat{y} - \epsilon L_x \frac{\partial f(y,z)}{\partial z} \hat{z} \quad (16)$$

and when equation (16) is used in equation (15), the result is

$$\left[\frac{\partial p}{\partial x} - \epsilon L_x \frac{\partial f(y,z)}{\partial y} \frac{\partial p}{\partial y} - \epsilon L_y \frac{\partial f(y,z)}{\partial z} \frac{\partial p}{\partial z} \right]_{x=L_x [1 + \epsilon f(y,z)]} = 0 \quad (17)$$

Applying a Taylor-series expansion for p evaluated at the real boundary $L_x [1 + \epsilon f(y,z)]$ produces

$$\begin{aligned} p \Big|_{x=L_x [1 + \epsilon f(y,z)]} &= p \Big|_{x=L_x} + \frac{\partial p}{\partial x} \Big|_{x=L_x} \epsilon L_x f(y,z) \\ &+ \frac{1}{2} \frac{\partial^2 p}{\partial x^2} \Big|_{x=L_x} [\epsilon L_x f(y,z)]^2 + \dots \end{aligned} \quad (18)$$

Substituting equation (12) into the RHS of equation (18), taking the partial derivative with respect to x on both sides and keeping the first-order terms in ϵ , yields [Ref. 1]

$$\left. \frac{\partial p}{\partial x} \right|_{x=L_x [1 + \epsilon f(y,z)]} = \left. \frac{\partial p_0}{\partial x} \right|_{x=L_x} + \epsilon \left. \frac{\partial p'}{\partial x} \right|_{x=L_x} + \left. \frac{\partial^2 p_0}{\partial x^2} \right|_{x=L_x} \epsilon L_x f(y,z) + \dots \quad (19)$$

Taking the partial derivatives with respect to y and z and using exactly the same procedure gives [Ref. 1]

$$\left. \frac{\partial p}{\partial y} \right|_{x=L_x [1 + \epsilon f(y,z)]} = \left. \frac{\partial p_0}{\partial y} \right|_{x=L_x} + \epsilon \left. \frac{\partial p'}{\partial y} \right|_{x=L_x} + \left. \frac{\partial^2 p_0}{\partial y \partial x} \right|_{x=L_x} \epsilon L_x f(y,z) + \dots \quad (20)$$

$$\left. \frac{\partial p}{\partial z} \right|_{x=L_x [1 + \epsilon f(y,z)]} = \left. \frac{\partial p_0}{\partial z} \right|_{x=L_x} + \epsilon \left. \frac{\partial p'}{\partial z} \right|_{x=L_x} + \left. \frac{\partial^2 p_0}{\partial z \partial x} \right|_{x=L_x} \epsilon L_x f(y,z) + \dots \quad (21)$$

Substituting equations (19), (20), and (21) into equation (17) and keeping the first-order terms in ϵ results in

$$\left. \frac{\partial p'}{\partial x} \right|_{x=L_x} = L_x \left[-f(y,z) \frac{\partial^2 p_0}{\partial x^2} + \frac{\partial f(y,t)}{\partial y} \frac{\partial p_0}{\partial y} + \frac{\partial f(y,z)}{\partial z} \frac{\partial p_0}{\partial z} \right]_{x=L_x} \quad (22)$$

The RHS of equation (22) can be represented as a Fourier series in cosines, so that p' can be expressed as a summation of normal modes. Hence,

$$\left. \frac{\partial p'}{\partial x} \right|_{x=L_x} = \sum_{m=0}^{\infty} \sum_{l=0}^{\infty} a_{ml} \cos \frac{m\pi}{L_y} y \cos \frac{L\pi}{L_z} z \cos (\omega t + \theta) \quad (23)$$

or

$$\left. \frac{\partial p'}{\partial x} \right|_{x=L_x} = \sum_{m=0}^{\infty} \sum_{l=0}^{\infty} a_{ml} (0, m, l/w, \theta) \quad (24)$$

where

$$a_{00} = \frac{1}{L_y L_z} \int_0^{L_y} \int_0^{L_z} [G] dy dz \quad (25)$$

$$a_{m0} = \frac{2}{L_y L_z} \int_0^{L_y} \int_0^{L_z} [G] \cos \frac{m\pi}{L_y} y dy dz \quad (26)$$

$$a_{0l} = \frac{2}{L_y L_z} \int_0^{L_y} \int_0^{L_z} [G] \cos \frac{L\pi}{L_z} z dy dz \quad (27)$$

$$a_{ml} = \frac{4}{L_y L_z} \int_0^{L_y} \int_0^{L_z} [G] \cos \frac{m\pi}{L_y} y \cos \frac{L\pi}{L_z} z dy dz, \quad \begin{matrix} m \neq 0 \\ n \neq 0 \end{matrix} \quad (28)$$

and G is defined as

$$G \equiv \left. \frac{\partial p'}{\partial x} \right|_{x=L_x} \quad (29)$$

In order to find the contribution to p' from each of the terms, it is stated [Ref. 16] that, for a cavity forced by a dynamic boundary condition at a boundary,

$$C_p^2 - L^2 p' = 0 \quad (30)$$

and the dynamic boundary condition from the (m, l) th term is

$$\left. \frac{\partial p'_{ml}}{\partial x} \right|_{x=L_x} = A \cos \frac{m\pi}{L_y} y \cos \frac{L\pi}{L_z} z e^{i(\omega t + Q)} \quad (31)$$

then

$$p'_{ml} = -A \frac{1}{\left(\frac{\omega}{C_0}\right)^2 L_x} \sum_{n=0}^{\infty} \Delta_n (-1)^n S_{nml} \cos \frac{n\pi}{L_x} x \cos \frac{m\pi}{L_y} y \cos \frac{L\pi}{L_z} z e^{i(\omega t + Q + \sigma_{nml})} \quad (32)$$

where

$$\Delta_n = \begin{cases} 1 & \text{if } n = 0 \\ 2 & \text{if } n = 1, 2, 3, \dots \end{cases}$$

Applying this solution to equation (24) gives the complete solution for the first-order perturbation [Ref. 6]

$$p = (n, m, l / \omega, \theta) - \frac{\epsilon}{\left(\frac{\omega}{C_0}\right)^2 L_x} \sum_{\substack{n=0 \\ m=0 \\ l=0}}^{\infty} a_{nml} \Delta_n (-1)^n S_{nml} (n, m, l / \omega, \theta + \sigma_{nml}) \quad (33)$$

As it is stated [Ref. 16], if this is near a resonance, $\omega \sim \omega_{nml}$, then this term will dominate the summation and all other non-degenerate terms can be omitted. Consequently, equation (33) becomes

$$p = (n, m, l / \omega, \theta) - \frac{\epsilon}{\left(\frac{\omega}{C_0}\right)^2 L_x} a_{nml} \Delta_n (-1)^n S_{nml} (n, m, l / \omega, \theta + \sigma_{nml}) \dots \quad (34)$$

III. EXPERIMENTAL CONSIDERATIONS

A. COMPUTER-CONTROLLED APPARATUS

The rectangular cavity used in this research was designed and constructed in 1977 by Kuntsal [Ref. 6] (Figure 1). One wall of the cavity could be moved and secured. The interior of the cavity was 12.002 inches long and 2.502 inches high, while the width could be varied from approximately 5.50 inches to 7.00 inches, in 0.25-inch steps. The piston, located in a 2.25-inch diameter port in the floor of the cavity, was supported by an O-ring to produce a seal between the piston and the port. Three 1/4-inch diameter microphone ports were used. A condenser microphone was mounted in a 0.24-inch aluminum case and an O-ring and silicon grease were used between this case and the ports for sealing.

Modal designation for the lowest three modes is shown in Figure 2. The (020) and (100) modes are nearly degenerate. The (020) mode is a one-dimensional standing wave with nodes 3 and 9 inches along the long wall of the cavity and the (100) mode is a standing wave with one node in the middle of the short wall. When the microphone is placed at position A, the (100) mode is sensed without contamination from the (020) mode. In position C, the (020) mode is sensed without contamination from the (100) mode. A block diagram of the apparatus is shown in Figure 3.

The piston was driven by an M-B Electronics model EA1500 exciter, which in turn was driven by an APS Electronic model 114

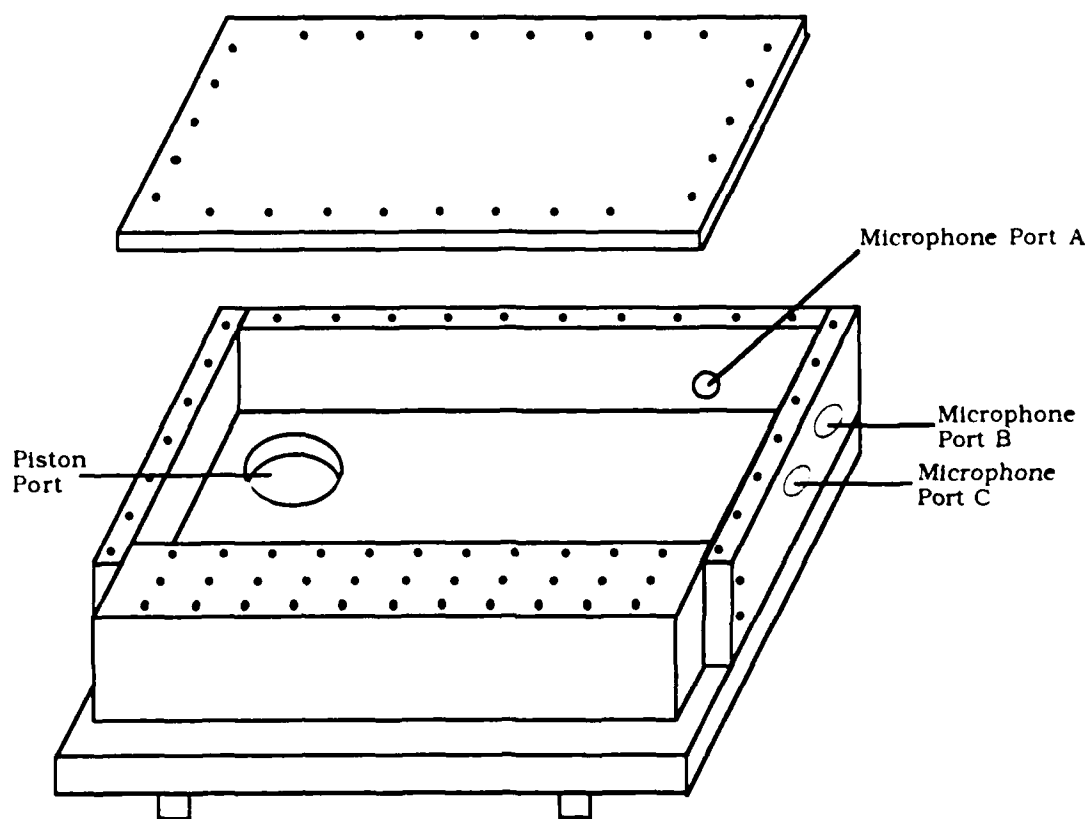
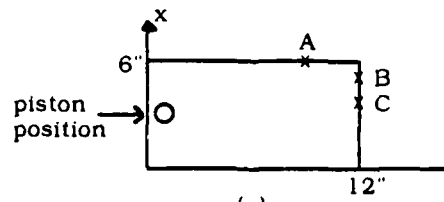
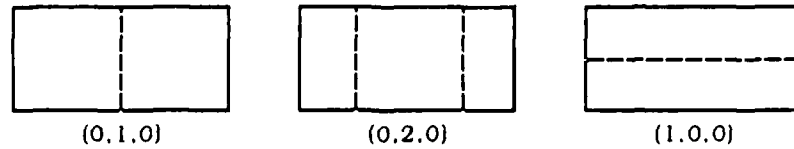


Figure 1
Rectangular Cavity



(a)



(b)

Figure 2

(a) Cavity Orientation

(b) Modal Designation

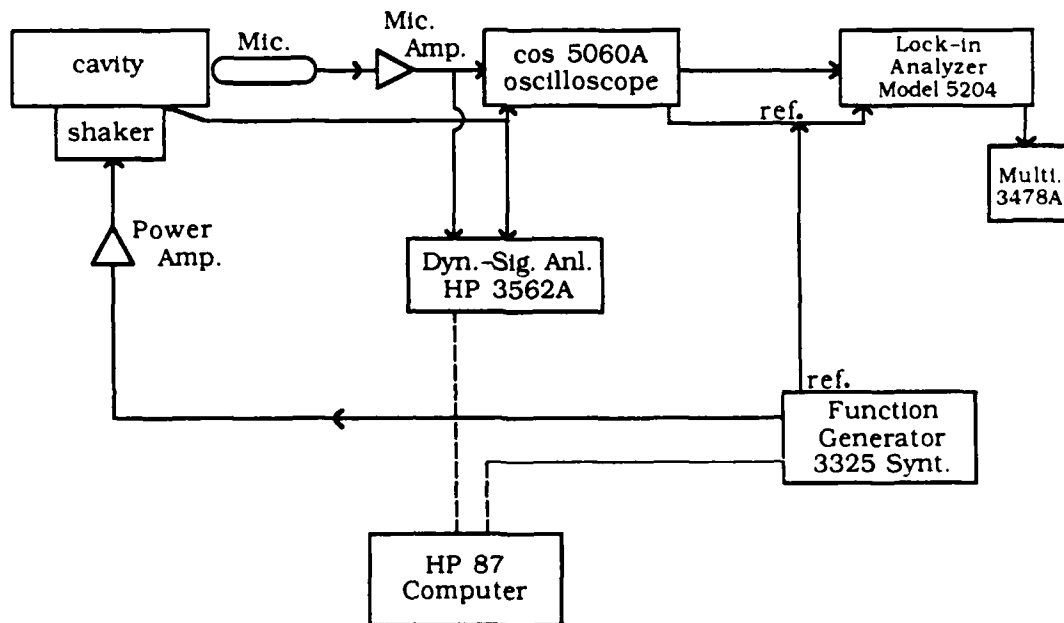


Figure 3

Block Diagram

power amplifier. The driving signal was produced by an HP 3325A Synthesizer/Function generator.

The piston movement was continuously analyzed by an Endevco model 2215 Accelerometer mounted within the piston. The output voltage of the microphone and output voltage of the accelerometer were measured by an HP 3678 multimeter. An HP 3562A Dynamic Signal analyzer was used to measure the harmonic distortion. A model 5204 Lock-in Analyzer was used to measure the resonance frequencies at small signal amplitude.

The sound pressure in the cavity was sensed by a Bruel and Kjaer 4136 condenser microphone with matching preamplifier 2807. The output of this preamplifier went to three pieces of equipment: (1) an HP 3478 multimeter to measure the voltage level, (2) an HP 3562A Dynamic Signal Analyzer to measure the harmonics, and (3) a Cos 5060A oscilloscope to monitor the undesired distortion of the accelerometer signal.

The HP 3562A Dynamic Signal Analyzer and HP 3325A Synthesizer/Function generator were controlled by an HP 87 computer. Two types of geometrical perturbations were used:

- a. The long wall was machined at a small angle (as shown in Figure 4).
- b. The long wall was machined as shown in Figure 5.

The effect of these geometrical perturbations on the resonance frequency of the (100) mode could be estimated by calculating an "effective" width $L_e = L - \Delta L$ of the perturbed cavity where $\Delta L = V/A$

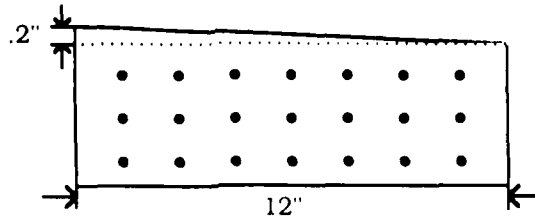


Figure 4

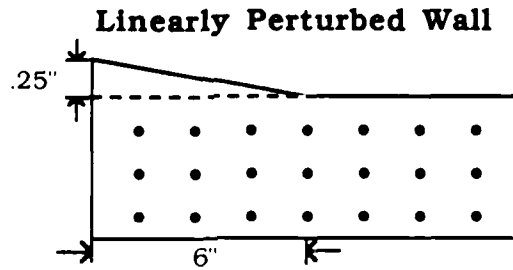


Figure 5

Wedged Perturbation

and V and A are the volume and cross-sectional area of the perturbation. [Ref. 1]

B. STRENGTH PARAMETER (STRM)

Strength of the finite amplitude interaction is characterized by the strength parameter STRM [Ref. 6].

$STRM = M\beta Q_1$ where Q_1 is the quality factor of the driven mode

$$\beta = \frac{1}{2} \left(1 + \frac{C_p}{C_v} \right) = 1.2 \text{ for air}$$

$$M = \frac{P_1}{\rho C^2}$$

$$P_1 = \frac{v_1 \sqrt{2}}{S_M}$$

where S_M is the microphone sensitivity.

The microphone output voltage v_1 is read on an HP 3562A Dynamic Signal Analyzer set at the fundamental harmonic. Microphone sensitivity was obtained with a Bruel and Kjaer model 4220 piston phone.

$$S_M = (1.56 \pm 0.03) \times 10^{-3} \text{ volt}/(\text{N}/\text{M}^2)$$

By using $\rho = 1.293 \text{ kg}/\text{m}^3$ and $C = 345 \text{ m}/\text{sec}$, we found

$$\text{STRM} = 7.07 \times 10^{-3} \times V \times Q. \quad (35)$$

This is the same sensitivity as is measured by Kuntsal [Ref. 6].

C. FREQUENCY PARAMETER (FP)

The frequency parameter is defined by

$$\text{FP} = 2Q_1 (\omega - \omega_1)/\omega_1 \quad (36)$$

where f is a driving resonance frequency and f_1 is a resonance frequency of (010) mode. It is assumed that $\frac{\Delta\omega_n}{\omega_n} \ll 1$. FP indicates where the driving frequency is with respect to the fundamental resonance frequency of the cavity. As $|\text{FP}|$ increases, the nonlinear effects will in general become smaller for a given strength parameter.

D. HARMONICITY COEFFICIENT (E(n))

The harmonicity coefficient is defined as [Ref. 6]

$$E(n) = \frac{\omega_n - n\omega_1}{n\omega_1} \quad (37)$$

$E(n)$ characterizes how well the modes of a given family are tuned.

E. COMPUTER PROGRAMS

Two computer programs were developed. The first program finds the resonance frequencies and calculates the quality factors (Figure 6). The second program drives the Dynamic Signal Analyzer HP 3562A by a HP 3325A Synthesizer/Function generator and finds and calculates harmonic content of the microphone output at each driving frequency (Figure 7).

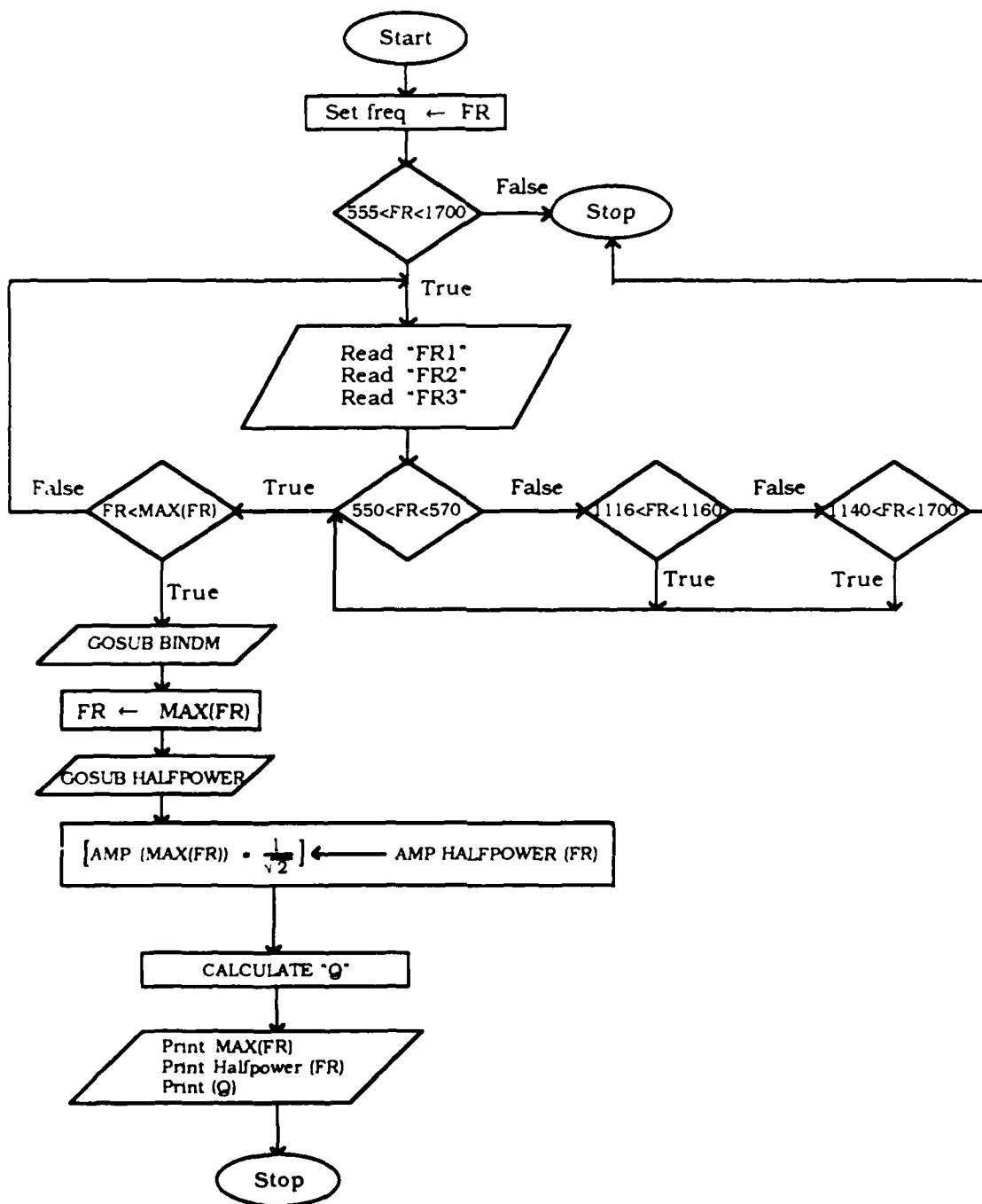


Figure 6
"Q" Calculation Flow Diagram

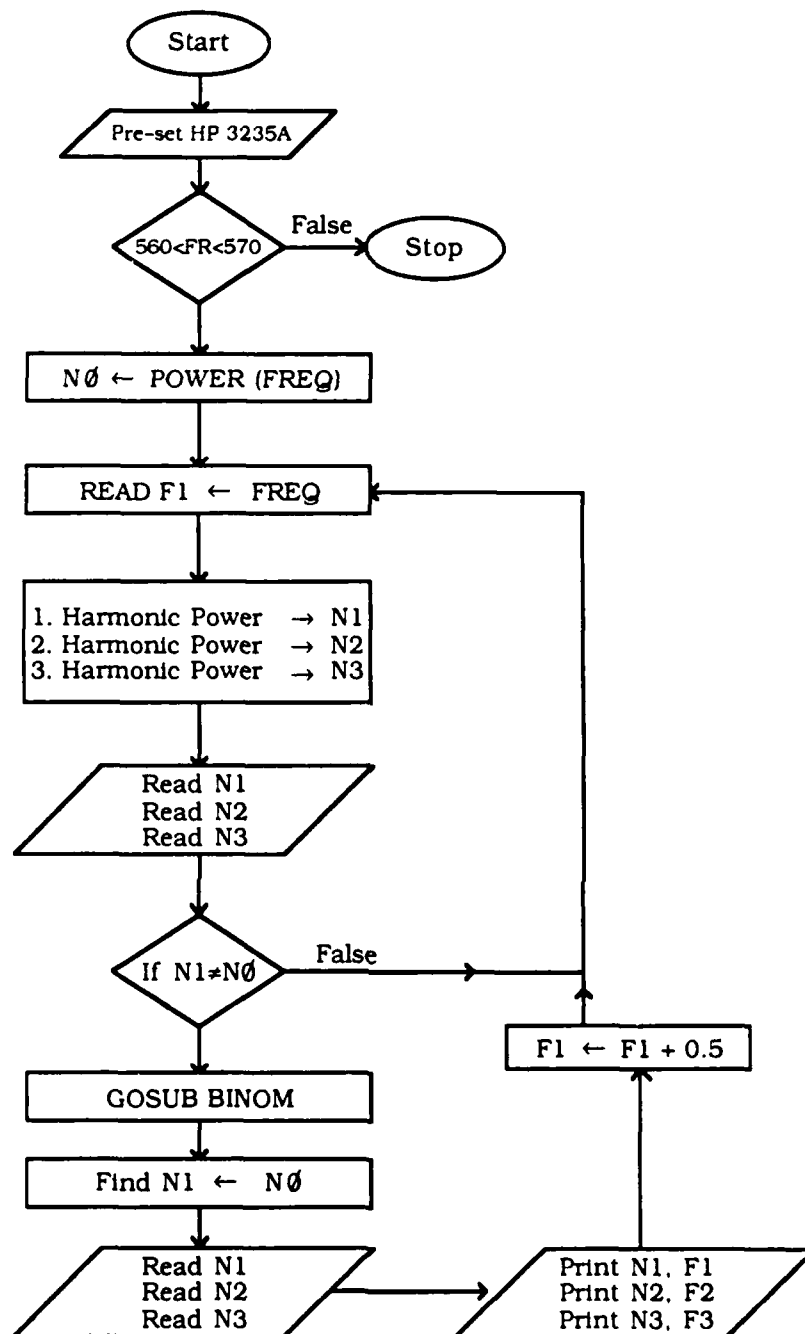


Figure 7

Power of the Harmonic Content Calculation Flow Diagram

IV. DATA COLLECTION PROCEDURES

A. SYSTEM ALIGNMENT

The primary factor in setting the lower limit to the measurement of harmonic content was the amount of distortion injected into the cavity by the piston. Misalignment of the piston within its port causes distortion of the piston motion which was detected by analyzing the harmonic content of the accelerometer output voltage. (With the piston removed from its port, distortion levels were of the same order of magnitude as the general electronic noise level of the accelerometer system when at rest.) Before each run, the piston was aligned within its port so that the accelerometer output voltage contained less than 0.1 percent second harmonic and 0.2 percent third harmonic.

After testing various configurations, the one selected for ease of alignment consisted of the cavity mounted on a tripod support directly above the exciter, which was supported by its own base in an upright position. Both the cavity tripod and the exciter rested on a 5/16-inch pad of stiff acoustic rubber. Once the system was aligned, only an occasional minor adjustment was necessary to maintain low piston distortion.

B. AUTOMATIC DATA COLLECTION

Since the resonance frequencies of the cavity were observed to drift with time, the system was allowed to warm up for at least three hours prior to data collection. The harmonic content of the accelerometer output was analyzed and the piston was adjusted until

the second harmonic of the accelerometer output was at least 50 dB below that of the fundamental frequency. Figure 8 shows the drift in f_r is approximately linear in time.

Data was collected using two measurement procedures in the computer programs: (1) a pre- and post-run infinitesimal amplitude measurement; and (2) the finite amplitude measurement.

1. Pre-Run and Post-Run Infinitesimal Amplitude Measurements

During the pre-run and post-run infinitesimal amplitude measurement, the piston was driven 80 mV (rms). Because the (100) and (020) modes were nearly degenerate, measurements of the properties of the (100) mode were made with the microphone in port C while measurements of the (020) mode were made with the microphone in port B. The resonant frequency of the fundamental and the Q factor first few (0,n,0) in the modes were determined from

$$f_r = \frac{f_u - f_L}{2} \quad (38)$$

$$Q = \frac{f_r}{f_u - f_L} \quad (39)$$

and the harmonicity coefficients were then calculated from

$$E_n = \frac{f_n - nf_1}{nf_1} \quad (40)$$

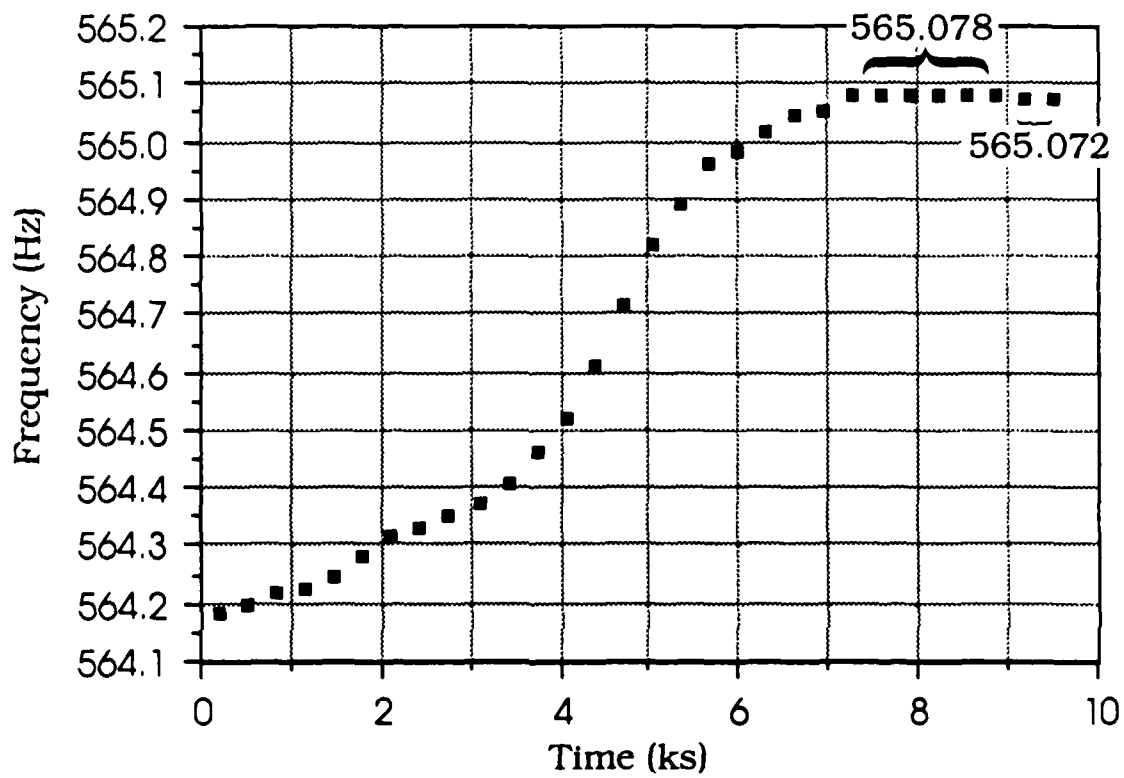


Figure 8
Drift in Frequency

where f_u and f_L are the frequencies of the upper and lower half-power points, and f_n is the resonance frequency of the n th member of the (010) family. Figure 9 shows the precision of frequency measurements.

2. The Finite-Amplitude Measurement

All finite-amplitude measurements were made at port B. Throughout this measurement, V_1 had to be kept constant by the computer program (Appendix C), which required adjustment of the driving voltage applied to the piston. The frequency was increased by the computer in 0.5-Hz steps through ± 5 Hz about the resonance frequency of a fundamental mode. At each driving frequency, the harmonic content of the microphone output, usually up to the fourth, was measured with the HP 3562A Dynamic Signal analyzer.

To determine the exact value of the frequency parameter, the value of f_r at the instant of the measurement of V_n was determined from the first computer program.

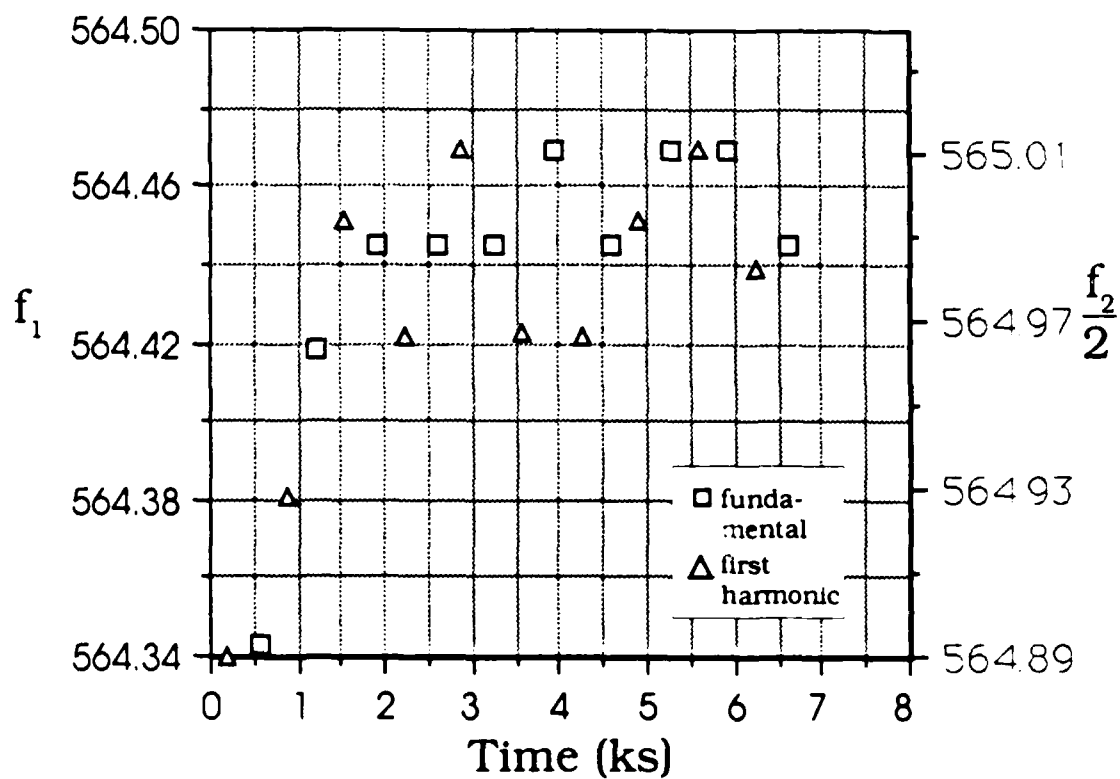


Figure 9
Precision of Frequency Measurements

V. RESULTS

In this section, the theoretical predictions and experimental results obtained by Kuntsal [Ref. 6] will be qualitatively compared to the experimental results obtained by using the computer-controlled equipment.

The information on the empirical losses and resonance frequencies is contained in the Q 's and E 's. It is important to note that, because V_1 is always kept constant as a function of frequency, the second harmonic distortion is maximized for $\omega = \omega_2/2$. The point where this occurs for each V_2/V_1 curve is indicated by an arrow with the label F_{020} . At that point, the value of the frequency parameter is

$$F_{020} = 2 Q_{010} E_{020}$$

Similarly,

$$F_{030} = 2 Q_{010} E_{030}$$

is indicated on each graph. The arrow labelled F_{100} indicates the position where the nearly degenerate (1,0,0) mode is resonant, and the value of F_{100} is

$$F_{100} = 2 Q_{010} E_{100}$$

The theoretical predictions for unperturbed cavities made by Kuntsal [Ref. 6] were compared to the experimental results as seen in

Figure A. It is clearly seen that the theory and experiment are qualitatively in agreement.

At Figure 9, f_1 and f_2 are plotted as a function of time. This figure showed two things: (1) changes of resonance frequencies of the family modes are proportional to the frequency, as would be expected if the long dimension of the cavity changes with time, most likely due to temperature changes; and (2) the fluctuations of resonance frequencies from measurement to measurement indicate a precision of ± 0.02 Hz in determining the resonance frequencies of the lowest mode. By using the value of ± 0.02 Hz, expected uncertainties in the E's are

$$\Delta E_{\text{expected}} = \frac{f_n \pm 0.02 - n(f_1 \pm 0.02)}{nf_1}$$

Calculated $\Delta E_{\text{expected}}$ and measured ΔE 's between pre- and post-run are tabulated in Table 4. The difference of the pre-run and post-run E's for the family modes in the unperturbed cavity are within the expected precision. For the 100 mode (non-family mode), this difference is much greater than expected, indicating that the cavity may be changing its dimensions unequally in all directions.

For a linear perturbation (Figure B) and for the wedge perturbation (Figure C), the harmonic content in Reference 6 is in qualitative agreement with experiment, considering that lower Q's and different E's were observed compared to Kuntsal's measurement [Ref. 6].

VI. CONCLUSIONS

The experimental apparatus, procedures, and computer programs are capable of providing data sufficiently precise to test the prediction of the theory in the absence and presence of geometrical perturbation.

Because the strength parameters (STRM) and quality factors (Q) calculated in the experiment did not match the STRM and Q in Reference 6, quantitative agreement could not be tested. However, the experimental results show that a geometrical perturbation alters the finite amplitude behavior of the cavity, and that the nature of these changes is in qualitative agreement with the predictions of the theory.

The quantitative disagreements between the theory and experiment for the perturbed cavities may be because the resonance frequency of the non-family mode is not tracking the family modes.

In order to avoid disturbing the position of the piston in the port of the cavity, the microphone has to be shifted very carefully from one port to another between the "pauses" as the program goes on.

APPENDIX A

CURVES

Average Values for Q_s and E_s		
Mode: 010	$Q_1 = 194.72$	$E_1 = 0.0$
STRM: .389	$Q_2 = 278.26$	$E_2 = 96.08 \times 10^{-5}$
	$Q_3 = 355.18$	$E_3 = 16.86 \times 10^{-4}$
	$Q_{100} = 263.12$	$E_{100} = 82.67 \times 10^{-5}$

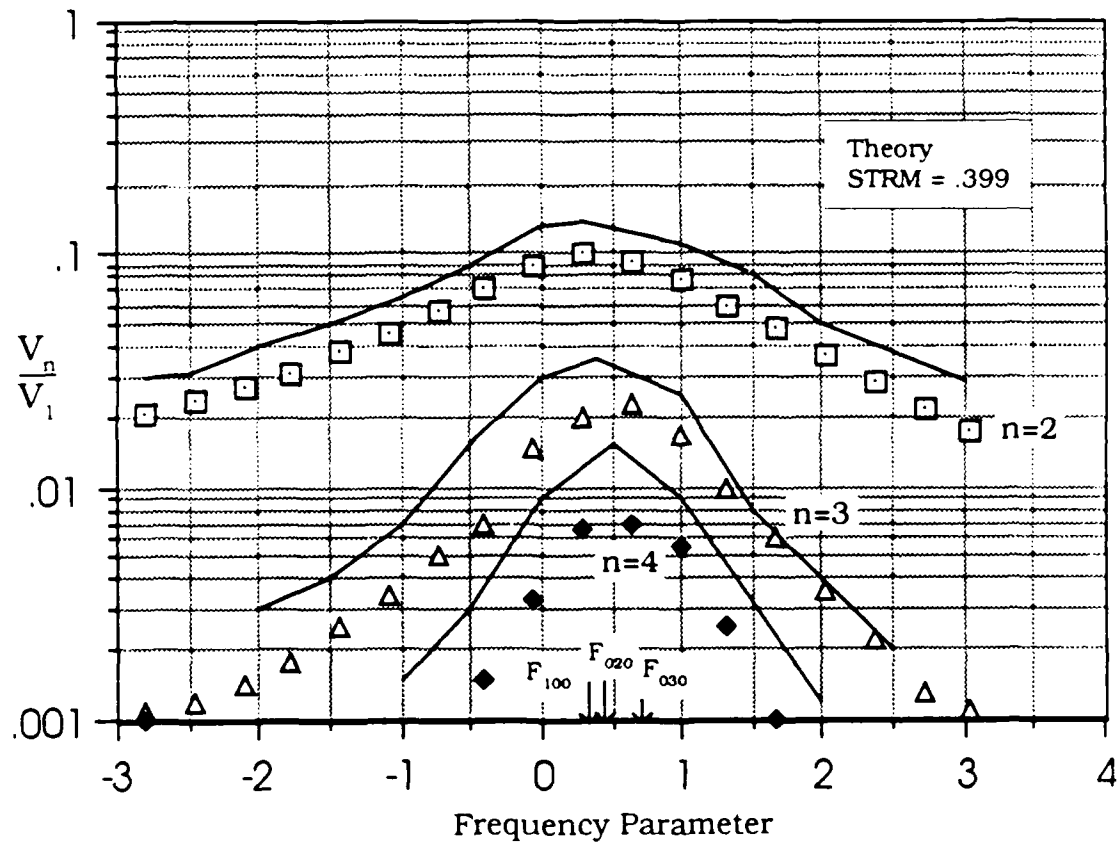


Figure A
Unperturbed Cavity

Average Values for Q_s and E_s					
Mode: 010	$Q_1 = 192.81$	$E_1 = 0.0$			
STRM: .355	$Q_2 = 287.86$	$E_2 = 20.39 \times 10^{-4}$			
	$Q_3 = 340.61$	$E_3 = 30.70 \times 10^{-4}$			
	$Q_{100} = 262.99$	$E_{100} = 23.75 \times 10^{-4}$			

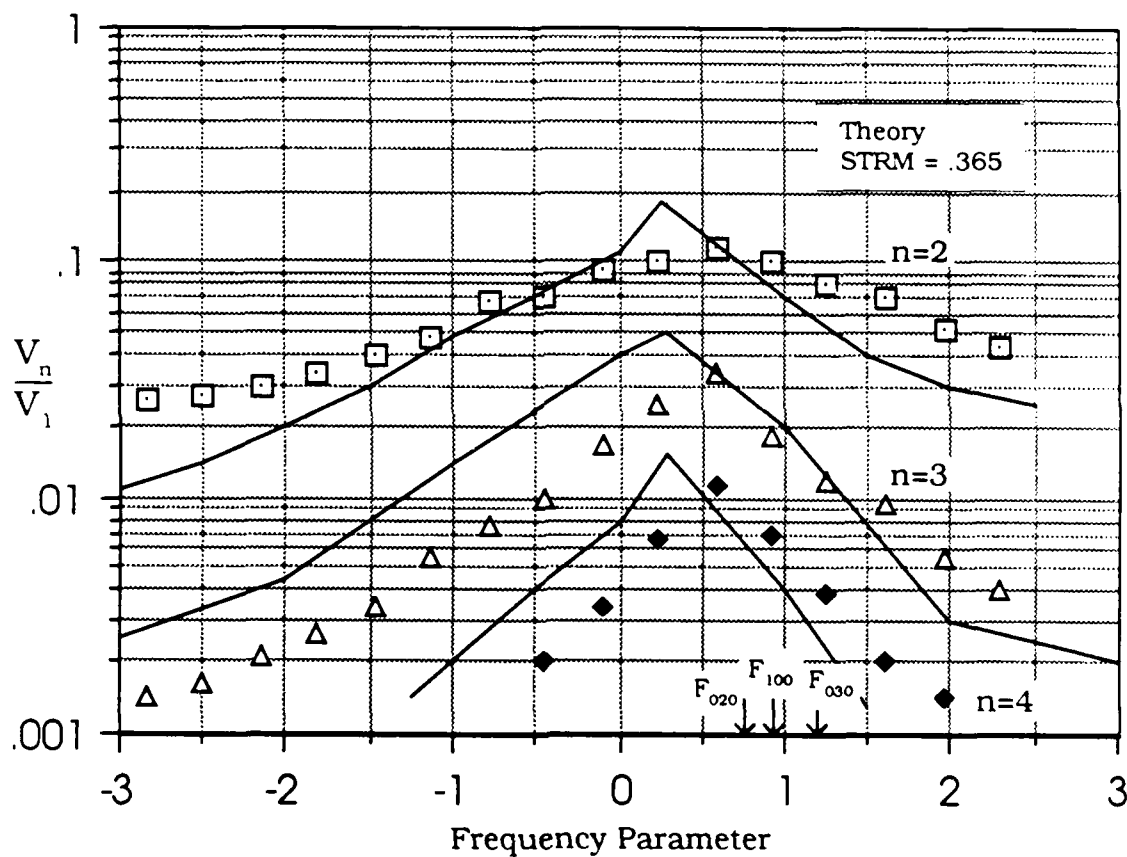


Figure B
Linear Perturbed Cavity

Average Values for Qs and Es		
Mode: 010	$Q_1 = 187.52$	$E_1 = 0.0$
STRM: .370	$Q_2 = 288.13$	$E_2 = -49.02 \times 10^{-4}$
	$Q_3 = 350.42$	$E_3 = -23.25 \times 10^{-4}$
	$Q_{100} = 291.40$	$E_{100} = -51.34 \times 10^{-4}$

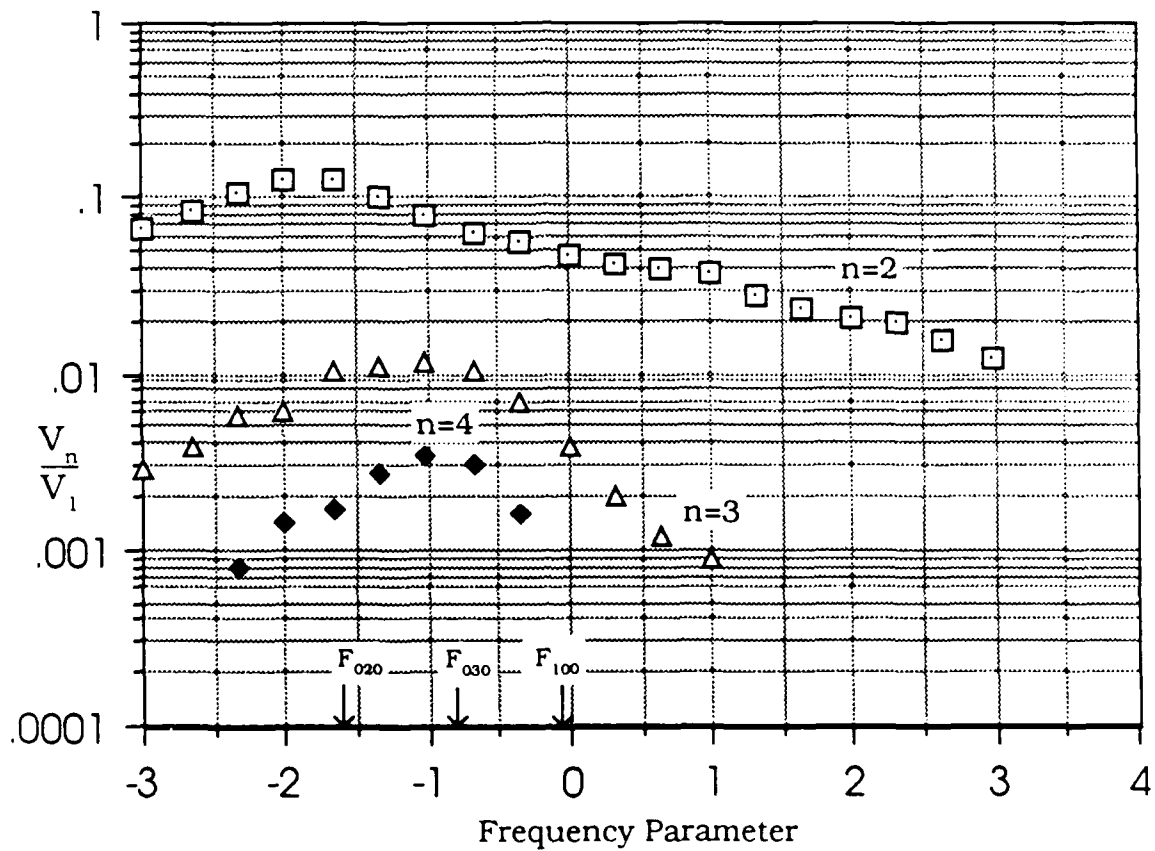


Figure C

Wedge Perturbed Cavity

APPENDIX B

TABLES

TABLE 1

UNPERTURBED CAVITY

(SEE FIGURE A)

Pre-Run

Mode	f_u	f_L	f_r	Q	E
010	565.801	562.875	564.351	195.40	0.0
020	1131.840	1127.791	1129.812	278.69	98.16×10^{-5}
030	1698.271	1693.524	1695.901	356.51	16.82×10^{-4}
100	1131.872	1127.590	1129.731	264.20	91.17×10^{-5}

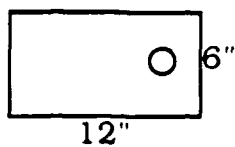
Finite-Amplitude Run

$V_1 = -11$ dB

Mode: 010

STRM = .389

f (Hz)	V_2 (dB)	V_3 (dB)	V_4 (dB)	V_2/V_1	V_3/V_1	V_4/V_1	FP
558.5	-50.0	-70.5	-70.5	0.0113	0.0014	0.0012	-4.19
559.0	-47.9	-72.0	-69.0	0.0143	0.0013	0.0011	-3.85
559.5	-46.9	-73.8	-67.8	0.0160	-	0.0011	-3.50
560.0	-46.0	-72.6	-67.5	0.0179	-	0.0010	-3.15
560.5	-44.8	-71.2	-69.7	0.0204	0.0011	0.0010	-2.81
561.0	-43.7	-69.7	-73.5	0.0233	0.0012	-	-2.47
561.5	-42.4	-67.8	-76.5	0.0269	0.0014	-	-2.12
562.0	-41.0	-65.7	-75.9	0.0316	0.0018	-	-1.78
562.5	-39.4	-63.2	-82.5	0.0380	0.0025	-	-1.43
563.0	-37.8	-60.3	-85.0	0.0457	0.0034	-	-1.09
563.5	-35.9	-56.6	-74.9	0.0569	0.0052	-	-0.74
564.0	-34.0	-52.2	-67.5	0.0708	0.0070	0.0015	-0.40
564.5	-32.2	-47.6	-60.6	0.0876	0.0148	0.0033	-0.05
565.0	-31.1	-45.0	-54.5	0.0994	0.0200	0.0067	0.29
565.5	-31.6	-43.9	-52.9	0.0933	0.0226	0.0070	0.64
566.0	-33.3	-46.7	-56.0	0.0772	0.0164	0.0056	0.98
566.5	-35.3	-51.0	-63.2	0.0610	0.0100	0.0025	1.33
567.0	-37.6	-55.5	-70.8	0.0484	0.0060	0.0010	1.67
567.5	-39.8	-60.0	-73.6	0.0365	0.0036	-	2.02
568.0	-42.1	-64.3	-74.7	0.0279	0.0022	-	2.36
568.5	-44.1	-68.5	-74.2	0.0221	0.0013	-	2.71
569.0	-46.2	-69.5	-	0.0174	0.0011	-	3.05



Post-Run

Mode	f_u	f_L	f_r	Q	E
010	566.381	563.270	564.82	194.03	0.0
020	1132.740	1128.676	1130.71	277.82	94.00×10^{-5}
030	1699.770	1694.974	1697.37	353.84	16.90×10^{-4}
100	1132.800	1128.487	1130.64	262.03	74.16×10^{-5}

TABLE 2
LINEAR PERTURBATION CONFIGURATION
 (SEE FIGURE B)

Pre-Run

Mode	f_u	f_L	f_r	Q	E
010	569.465	566.545	565.653	193.72	0.0
020	1133.883	1129.961	1132.306	288.71	17.67×10^{-4}
030	1703.014	1698.008	1700.594	339.72	21.42×10^{-4}
100	1131.650	1131.341	1134.651	263.321	29.57×10^{-4}

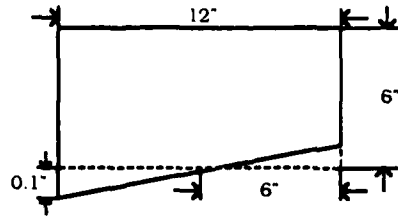
Finite-Amplitude Run

$V_1 = -12$ dB

Mode: 010

STRM = .355

f (Hz)	V_2 (dB)	V_3 (dB)	V_4 (dB)	V_2/V_1	V_3/V_1	V_4/V_1	FP
561.0	-43.0	-68.7	-	0.0251	0.0013	-	-3.19
561.5	-42.7	-68.0	-	0.0260	0.0014	-	-2.84
562.0	-42.3	-66.9	-	0.0271	0.0016	-	-2.50
562.5	-41.6	-64.5	-	0.0296	0.0021	-	-2.16
563.0	-40.3	-62.7	-	0.0342	0.0026	-	-1.82
563.5	-38.7	-60.1	-	0.0411	0.0035	-	-1.47
564.0	-37.3	-56.2	-	0.0485	0.0055	-	-1.13
564.5	-34.2	-53.5	-	0.0691	0.0075	-	-0.79
565.0	-33.8	-51.0	-65.0	0.0721	0.0100	0.0020	-0.44
565.5	-31.8	-46.4	-60.1	0.0911	0.0170	0.0035	-0.10
566.0	-30.9	-43.0	-54.6	0.1012	0.0251	0.0066	0.24
566.5	-29.6	-40.3	-50.0	0.1161	0.0344	0.0112	0.58
567.0	-30.9	-45.8	-54.1	0.1000	0.0180	0.0070	0.92
567.5	-32.8	-49.8	-59.2	0.0810	0.0115	0.0039	1.26
568.0	-34.1	-51.5	-65.0	0.0700	0.0094	0.0020	1.61
568.5	-36.7	-56.2	-68.1	0.0514	0.0055	0.0014	1.95
569.0	-38.0	-58.7	-	0.0441	0.0041	-	2.29



Post-Run

Mode	f_u	f_L	f_r	Q	E
010	570.410	567.456	566.861	191.90	0.0
020	1135.067	1131.116	1133.984	287.01	23.10×10^{-4}
030	1705.321	1700.340	1701.110	341.50	39.98×10^{-4}
100	1136.740	1132.416	1135.756	262.66	17.94×10^{-4}

TABLE 3
WEDGE PERTURBATION CONFIGURATION
(SEE FIGURE C)

Pre-Run

Mode	f_u	f_L	f_r	Q	E
010	566.912	563.864	565.381	185.80	0.0
020	1127.191	1123.281	1125.230	288.08	-48.92×10^{-4}
030	1695.310	1690.471	1692.891	349.27	-19.17×10^{-4}
100	1126.761	1122.911	1124.829	291.41	-52.47×10^{-4}

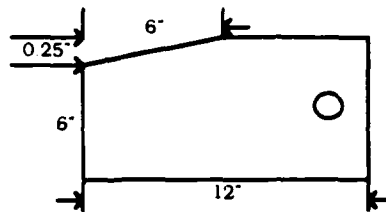
Finite-Amplitude Run

$V_1 = -11$ dB

Mode: 010

STRM = .370

f (Hz)	V ₂ (dB)	V ₃ (dB)	V ₄ (dB)	V ₂ /V ₁	V ₃ /V ₁	V ₄ /V ₁	FP
559.4	-39.5	-66.9	-	0.0376	0.0016	-	-3.99
559.9	-37.9	-65.3	-	0.0450	0.0019	-	-3.66
560.4	-36.4	-63.9	-	0.0540	0.0023	-	-3.33
560.9	-34.5	-61.8	-	0.0672	0.0029	-	-3.00
561.4	-32.4	-59.1	-78.0	0.0856	0.0039	-	-2.66
561.9	-30.3	-55.7	-72.7	0.1090	0.0058	0.0008	-2.33
562.4	-28.7	-55.6	-68.2	0.1310	0.0059	0.0014	-2.00
562.9	-28.9	-50.8	-65.3	0.1271	0.0103	0.0017	-1.67
563.4	-30.9	-50.0	-62.5	0.1010	0.0112	0.0027	-1.34
563.9	-32.3	-49.7	-60.3	0.0810	0.0116	0.0034	-1.01
564.4	-34.7	-50.9	-61.4	0.0650	0.0101	0.0030	-0.67
564.9	-36.3	-54.3	-67.0	0.0550	0.0068	0.0016	-0.34
565.4	-37.5	-59.3	-75.2	0.0480	0.0038	-	-0.01
565.9	-38.4	-65.0	-	0.0430	0.0020	-	0.32
566.4	-39.3	-69.7	-	0.0391	0.0012	-	0.65
566.9	-39.7	-72.2	-	0.0370	0.0009	-	0.98
567.4	-40.6	-74.5	-	0.0280	-	-	1.32
567.9	-40.7	-75.4	-	0.0230	-	-	1.65
568.4	-41.6	-73.5	-	0.0210	-	-	1.98
568.9	-44.0	-71.5	-	0.0193	-	-	2.31
569.4	-47.3	-70.9	-	0.0151	-	-	2.64
569.9	-49.1	-71.1	-	0.0120	-	-	2.97



Post-Run

Mode	f_u	f_L	f_r	Q	E
010	566.950	563.963	565.464	189.24	0.0
020	1127.311	1123.411	1125.371	288.18	-49.12×10^{-4}
030	1695.544	1690.731	1693.144	351.57	-27.33×10^{-4}
100	1126.981	1123.126	1125.051	291.39	-50.21×10^{-4}

TABLE 4
E'S DIFFERENCES BETWEEN RUNS

	Unperturbed Configuration	Linear Perturbed Configuration	Wedge Perturbed Configuration
ΔE_2	$.416 \times 10^{-4}$	5.43×10^{-4}	0.2×10^{-4}
ΔE_3	$.08 \times 10^{-4}$	8.56×10^{-4}	8.16×10^{-4}
ΔE_{100}	1.7×10^{-4}	11.63×10^{-4}	2.26×10^{-4}
$\Delta E_{\text{expected}}$	$.53 \times 10^{-4}$		

APPENDIX C

COMPUTER PROGRAMS

This program drives the HP 3325A Synthesizer/Function generator between 562 Hz and 1710 Hz, finds the resonance frequency, and calculates the quality factor (Q).

```
10  ! SUBROUTINE Q
14  SETTIME 0,87200
15  FOR INC=1 TO 30
20  K=-1
30  FOR FREQ=562 TO 1710 STEP 2
50  IF FREQ>550 AND FREQ<570 THEN GOTO 210
70  IF FREQ>570 THEN GOTO 90
90  FOR FREQ=1116 TO 1140 STEP 2
110 IF FREQ>1115 AND FREQ<1140 THEN GOTO 210
130 IF FRQ>1140 THEN GOTO 1791
140 K=K+1
150 FOR FREQ=1680 TO 1710 STEP 2
170 IF FREQ>1670 AND FREQ<1710 THEN GOTO 210
190 IF FREQ>1710 THEN GOTO 1800
210 F1=FREQ
230 F2=F1+2
250 F3=F1+4
270 REMOTE 717,723,702
290 OUTPUT 717 ;"FR";F1;"HZ"
310 WAIT 5000
330 ENTER 723 ; AMP1
350 OUTPUT 717 ;"FR";F2;"HZ"
370 WAIT 5000
390 ENTER 723 ; AMP2
410 OUTPUT 717 ;"FR";F3;"HZ"
430 WAIT 5000
450 ENTER 723 ; AMP3
470 DISP F1,F2,F3,AMP1,AMP2,AMP3,K
510 IF AMP2<AMP1 OR AMP2<AMP3 THEN GOTO 590
570 IF AMP2>AMP1 OR AMP2>AMP3 THEN GOSUB BINOM
590 NEXT FREQ
610 ! SUBROUTINE BINOM
```

```

630  BINOM:
650  P=F2
670  S=2
690  S=S/2
710  OUTPUT 717 ;"FR";P;"HZ"
720  WAIT 5000
730  ENTER 723 ; AP
750  IF P>1710 THEN GOTO 1800
770  PU=P+S
790  OUTPUT 717 ;"FR";PU;"HZ"
800  WAIT 5000
810  ENTER 723 ; AU
830  PL=P-S
850  OUTPUT 717 ;"FR";PL;"HZ"
860  WAIT 5000
870  ENTER 723 ; AL
890  DISP P,PU,PL,AP,AU,AL
910  IF AU>AP THEN P=PU
930  IF AL>AP THEN P=PL
950  IF S>.008 THEN GOTO 690
970  GOSUB HPWR
990  RETURN
1010 ! SUBROUTINE HALFPOWER
1030 HPWR:
1050 DISP P,AP
1060 DISP TIME
1065 PRINT TIME
1070 PRINT "MAX"
1090 PRINT P,AP
1100 IF INC>1 AND INC<30 THEN GOTO 1771 ELSE GOTO 1110
1110 PRINT "REAL HALFPOWER"
1130 APH1=AP/2^.5
1150 PRINT APH1
1170 FOR F=1 TO 2
1190 PH=P+((-1)^F)
1210 OUTPUT 717 ;"FR";PH;"HZ"
1230 WAIT 5000
1250 ENTER 723 ; AH
1270 DISP PH,AH
1290 IF AH<APH1 THEN GOTO 1350 ELSE GOTO 1310
1310 PH=PH+((-1)^F)
1330 GOTO 1210
1350 S=.5
1370 PHI=PH-(S*((-1)^F))
1390 FOR I=1 TO 10
1410 OUTPUT 717 ;"FR";PHI;"HZ"
1430 WAIT 5000

```

```

1450 ENTER 723 ; AHI
1470 S=S/2
1490 IF AHI>APH1 THEN GOTO 1570
1510 PHI=PHI-(S*((-1)^F))
1530 NEXT I
1550 GOTO 1610
1570 PHI=PHI+(S*((-1)^F))
1590 NEXT I
1610 PRINT "HALFPOWER"
1630 DISP PHI,AHI
1650 PRINT PHI,AHI
1670 IF F=1 THEN PHIR=PHI
1960 NEXT F
1710 Q=P/(PHI-PHIR)
1730 PRINT "Q VALUE"
1750 PRINT Q
1770 DISP Q
1771 K=K+1
1772 IF K=0 THEN GOTO 90
1773 ! AFTER FIRST PAUSE SHIFT THE MICROPHONE TO THE PORT C TO
      MEASURE THE FREQUENCY OF THE DEGENERATE MODE.
1775 ! AFTER SECOND PAUSE SHIFT THE MICROPHONE TO THE PORT B
1791 IF K=1 THEN PAUSE
1792 IF K=2 THEN PAUSE
1793 IF K=1 THEN GOTO 90
1794 IF K=2 THEN GOTO 140
1797 RETURN
1800 NEXT INC
1810 END

```

This program drives the HP 3562A Dynamic SignalAnalyzer by HP 3325A Synthesizer/Function generator and finds and computes the harmonic content of the microphone output at each driving frequency between 563 Hz and 570 Hz.

```

10  REMOTE 720,717
15  SETTIME 0,87033
20  OUTPUT 720 ;"PRST"
30  OUTPUT 720 ;"B"
40  OUTPUT 720 ;"FRS3KHZ"
50  OUTPUT 720 ;"PSPC"
60  P=800
70  OUTPUT 717 ;"AMP";P;"MV"
80  OUTPUT 720 ;"LNRS"
100 OUTPUT 720 ;"STBL"
110 OUTPUT 720 ;"PSP2"
120 OUTPUT 720 ;"KEY31 "
125 ! DRIVING THE DYNAMIC SIGNAL ANALYZER AND READING THE
    HARMONIC CONTENT OF THE DRIVING FREQUENCY.
130 FREQ=563
140 OUTPUT 717 ;"FR";FREQ;"HZ"
150 OUTPUT 720 ;" SF563HZ "
160 WAIT 3000
170 OUTPUT 720 ;"STRT"
180 WAIT 8000
190 OUTPUT 720 ;"MKPK"
200 OUTPUT 720 ;"RDMK"
210 ENTER 720 ; X1,YB
220 DIL=YB
230 DISP X1,DIL
234 PRINT TIME
235 PRINT X1,DIL
240 FOR FREQ=563 TO 570 STEP .5
250 OUTPUT 720 ;"FRS3KHZ"
251 OUTPUT 720 ;"SF";FREQ;"HZ"
255 OUTPUT 717 ;"FR";FREQ;"HZ"
260 FOR I=1 TO 4
270 OUTPUT 717 ;"AMP";P;"MV"
280 OUTPUT 720 ;"STRT"
290 WAIT 8000
300 OUTPUT 720 ;"MKPK"

```

```

310  OUTPUT 720 ;"RDMK"
320  ENTER 720 ; X,YB
324  DISP X,YB
325  PRINT X,YB
326  PRINT TIME
332  IF I=1 THEN GOTO 333 ELSE GOTO 350
333  IF FREQ>563 THEN GOTO 335 ELSE GOTO 350
335  GOSUB BINOM
350  OUTPUT 720 ;"SF";X+50;"HZ"
351  OUTPUT 720 ;" FRS.7KHZ"
355  NEXT I
356  NEXT FREQ
360  ! SUBROUTINE BINOM
365  ! THIS SUBROUTINE KEEPS THE FUNDAMENTAL CONSTANT.
370  BINOM:
380   $RAT=10^{(DIL/10)}/10^{(YB/10)}$ 
385  DISP RAT,DIL,YB
390  IF RAT>.999 AND RAT<1.001 THEN RETURN
400  P=P*RAT^.2
410  OUTPUT 717 ;"AMP";P;"MV"
420  OUTPUT 720 ;"STRT"
430  WAIT 8000
440  OUTPUT 720 ;"MKPK"
450  OUTPUT 720 ;"RDMK"
460  ENTER 720 ; X,YB
470  DISP X,YB
475  PRINT TIME
480  PRINT X,YB
490  IF FREQ>570 GOTO 660
510  GOTO 380
660  END

```

LIST OF REFERENCES

1. Coppens, A. B., private communication.
2. Sanders, J. V., private communication.
3. Lane, C., *Finite Amplitude Waves in a Rigid Walled Cavity*, Thesis, Naval Postgraduate School, Monterey, California, 1972.
4. DeVall, R. R., *Finite Amplitude Waves in Imperfect Cavities*, Thesis, Naval Postgraduate School, Monterey, California, 1973.
5. Slocum IV, W. S., *Finite Amplitude Standing Waves in Real Cavities Containing Degenerate Modes*, Thesis, Naval Postgraduate School, Monterey, California, 1975.
6. Kuntsal, E., *Finite Amplitude Standing Waves in Rectangular Cavities with Perturbed Boundaries*, Thesis, Naval Postgraduate School, Monterey, California, December 1978.
7. Kirchhoff, G., *Ann. Phys. Leipzig*, Vol. 134, pp. 177-193, 1868.
8. Lamb, H., *Dynamical Theory of Sound*, 2nd ed., Ch. 6, Edward Arnold and Co., London, England, 1925.
9. Fay, R. D., "Successful Method of Attack on Progressive Finite Waves," *J. Acoust. Soc. Am.*, Vol. 28, pp. 910-914, September 1956.
10. Keller, J. B., "Finite Amplitude Sound Produced by a Piston in a Closed Tube," *J. Acoust. Soc. Am.*, Vol. 26, pp. 253-254, 1954.
11. Keck, W., and R. T. Beyer, "Frequency Spectrum of Finite Amplitude Ultrasonic Waves in Liquids," *Phy. Fluids*, Vol. 3, pp. 346-352, 1960.
12. Coppens, A. B., and J. V. Sanders, "Finite Amplitude Standing Waves within Real Cavities," *J. Acoust. Soc. Am.*, 58 (6), December 1975.
13. Beech, W. L., *Finite Amplitude Standing Waves in Rigid Walled Tubes*, Thesis, Naval Postgraduate School, Monterey, California, 1967.

14. Ruff, P. G., *Finite Amplitude Standing Waves in Rigid Walled Tubes*. Thesis, Naval Postgraduate School, Monterey, California, 1967.
15. Kilmer, M. J. III, *Finite Amplitude Effects in Rectangular Cavities with Perturbed Boundaries*. Thesis, Naval Postgraduate School, Monterey, California, 1975.
16. Aydin, M., *Theoretical Study of Finite Amplitude Standing Waves in Rectangular Cavities with Perturbed Boundaries*. Thesis, Naval Postgraduate School, Monterey, California, 1978.

INITIAL DISTRIBUTION LIST

		<u>No. Copies</u>
1.	Defense Technical Information Center Cameron Station Alexandria, VA 22304-6145	2
2.	Library, Code 0142 Naval Postgraduate School Monterey, CA 93943-5002	2
3.	Deniz Kuvvetleri Komutanligi Bakanliklar, Ankara/Turkey	5
4.	Deniz Harp Okulu Komutanligi Kutuphanesi Tuzla, Istanbul/Turkey	1
5.	S. L. Garrett, Code 61GX Underwater Acoustics Naval Postgraduate School Monterey, CA 93943-5000	1
6.	Professor J. V. Sanders, Code 61Sd Physics Department Naval Postgraduate School Monterey, CA 93943-5000	1
7.	Professor A. B. Coppens, Code 61Cz Physics Department Naval Postgraduate School Monterey, CA 93943-5000	1
8.	LT R. D. Middleton, Jr. 141 John Street Hauppauge, NY 11787	1
9.	Ltjg Hakan Basaran Cemil Topuzlu Cad. Cinar Apt. No. 15/11 Fenerbahce, Istanbul/Turkey	3
10.	Chief of Naval Operations (Antisubmarine Warfare) Code OP-02 Washington D.C. 20350-2000	1

END

DATE

FILMED

DTIC

July 88